2024 IEEE/RSJ International Conference on Intelligent Robots and Systems (IROS)
October 14-18, 2024. Abu Dhabi, UAE

Identification of Flexible Joint Robot Inertia Matrix Using Frequency Response Analysis

Kiyoung Choi, Junho Song, Wonbum Yun, Deokjin Lee, and Sehoon Oh

***Abstract*— This paper presents a novel, nonlinearity robust identification method for deriving the inertia matrix of multi-DOF Flexible Joint Robots (FJR), utilizing resonance and anti-resonance frequencies in the Frequency Response Functions (FRF). Our proposed method overcomes the limitations of conventional approaches, which are susceptible to mechanical nonlinearities, leading to inaccurate models. By leveraging frequency domain techniques, our approach effectively mitigates the influence of nonlinear characteristics, providing a more accurate and reliable means of robot control. Furtermore, the paper highlights the benefits of frequency domain system identification, including nonlinear robustness and the ability to decompose the flexible joint into motor and load components. Finally, a novel sequential excitation algorithm is proposed to obtain the inertia matrix of a multi-DOF robot manipulator without relying on complex theories or optimizations. The effectiveness of the proposed algorithm is verified through simulation and experiment.**

I. INTRODUCTION

The precise control of robots, especially in scenarios where they operate in close proximity to humans, necessitates accurate models of their dynamic behavior. This is particularly critical for robots categorized as Flexible Joint Robots (FJR) [1], which are designed with intentional flexibility in their links and gears for impact protection and force measurement [2], [3]. While the flexibility of FJR offers the advantage of enabling safer interactions with humans, it introduces challenges due to its inherent oscillatory characteristics [4], [5], which can hinder achieving fast and precise control. Despite the development of various algorithms designed to enhance robot motion control in direct human contact [6], [7], a prevalent limitation remains: most control strategies depend on the accuracy of the dynamic model of the robot, which cannot be accomplished in real-world scenarios.

Several researchers have proposed methods for obtaining a dynamic model through robot parameter identification in time-domain [8], [9]. These methods involve formulating the robot's dynamic characteristics in the form of linear regression within the dynamic model equation. Subsequently, many researchers have developed methodologies based on Least-Square Estimation (LSE) for parameter estimation.

*This work was supported by the National Research Foundation of Korea(NRF) grant funded by the Korea government(MSIT) (No. RS-2024-00354028). It was also supported by the Technology Innovation Program (20011693) funded By the Ministry of Trade, Industry & Energy (MOTIE, Korea), the DGIST R&D Program of the Ministry of Science and ICT (23-PCOE-02).

K. Choi, J. Song, W. Yun, D. Lee, and S. Oh are the Department of Robotics and Mechatronics Engineering, DGIST, Daegu, 42988, Korea [kychoi, optimus120, dnjsqjadbs, djlee, and sehoon]@dgist.ac.kr

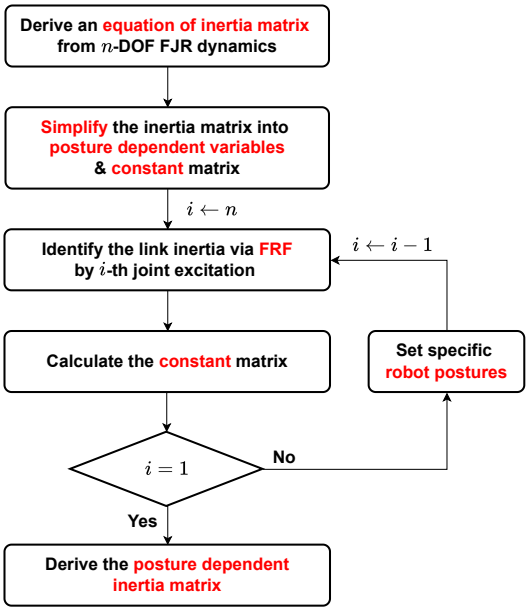

Fig. 1. Process of proposed sequential excitation algorithm.

Patrick et al. [10] proposed a method of using an optimization method to find a compromise between theoretical parameter values based on CAD data and obtained values through LSE. In addition, J. Swevers derived the excitation conditions for achieving optimal LSE-based parameter estimation, taking into account the specific regressor conditions of LSE [11]. Time-domain analysis, which analyzes the relationship between control inputs and outputs, struggles with two key limitations: significant influence from nonlinear effects like friction, and increased model complexity due to joint flexibility. These factors deteriorate the accuracy of parameter identification within the time domain, often resulting in an inaccurate model.

On the other hand, industrial applications of high-precision servo control has widely utilized system identification in the frequency domain [12]. In systems with noticeable vibration features, especially in cases like FJR where vibrations stand out, it is important to accurately investigate key parameters such as resonance frequency, anti-resonance frequency, and damping ratio. This is particularly significant for understanding the dynamics of such systems, which often requires using frequency response function (FRF)-based methods.

However, in robotics, using frequency-based methods to understand system dynamics comes with its own set of challenges. These include dealing with noise, nonlinearities, and the fact that robot dynamics can change depending on

parameters or posture. Despite these difficulties, several research projects have tried to tackle them using FRF analysis to find robot parameters [13]–[16]. But most of these studies focus on modeling and identifying parameters for single joints, rather than capturing the entire range of changing parameters for a multi-DOF manipulator. This limitation highlights the need for further research on applying FRF-based methods to identify the complete dynamics of multi-DOF robots.

This paper introduces a novel multi-DOF identification method, aimed at deriving the inertia matrix of multi-DOF FJR based on resonance and anti-resonance frequencies observed in the FRF such that it is less affected by nonlinearities. Unlike traditional approaches that primarily focus on time-domain methods susceptible to mechanical nonlinearities, our work proposes a novel identification strategy that leverages frequency domain techniques to mitigate the influence of nonlinear characteristics.

To achieve this goal, we outline our methodology for extracting crucial parameters of the FJR from frequency responses to ensure robust parameter identification. Next, we expand our innovative algorithm to determine the inertia matrix of a multi-degree-of-freedom (DOF) robot manipulator by strategically selecting postures and utilizing their mathematical formulation. To accomplish this, we employ a sequential excitation algorithm, stimulating each joint individually, starting from the farthest joint, and employing a Disturbance Observer (DOB) to treat the remaining links as single rigid bodies. Figure 1 visually illustrates the step-by-step system identification process. The contributions of this paper are detailed as follows:

- Novel parameter estimation method for FJR utilizing resonance and anti-resonance frequency of the FRF
- Decomposition of the inertia matrix into constants and time-varying variables and selection of postures for FRF measurements based on the decomposition
- Identification of the whole inertia matrix using sequential FRF measurements and DOB

II. Novel FJR Parameter Identification from Frequency Response Function

This section highlights our novel parameter identification methodology for the FJR which addresses challenges in parameter identifications.

A. Challenges in Parameter Identification of Robots

Robot motion is influenced by various mechanical nonlinearities, including friction. The effects of friction demonstrate a nonlinear dependency on velocity, typically modeled by the Stribeck curve, illustrated in Fig. 2(a). Moreover, stiction can even exhibit position dependency. Fig. 2(b) illustrates the control torque while the angular velocity of the actuator is maintained at 0.1 rad/s. The control torque, when the system operates at a constant velocity, can be interpreted as a measure of the actuator's frictional properties, which vary with position as shown in Fig. 2(b). Such variability primarily arises from factors such as cogging and ripple

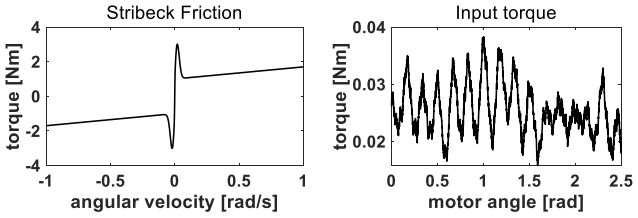

(a) (b)

Fig. 2. (a) Stribeck friction model. (b) The necessary torque to maintain the velocity of the motor.

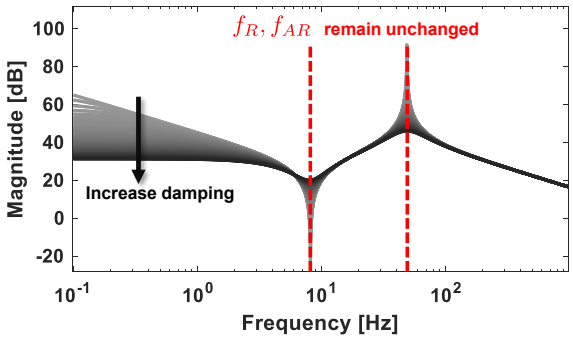

Fig. 3. FRF of a two mass system with various damping.

torque, indicating that the relationship between system input and output is disrupted by various influences. This poses a challenge for parameter identification algorithms.

Conventional approaches to parameter identification, encompassing both time and frequency domain analyses, heavily rely on the integrity of the input-output relationship. However, when this relationship is disrupted by the aforementioned factors, the accuracy of identification results is compromised.

Specifically, the magnitude of the FRF is susceptible to these influences. For instance, in Fig. 3, variations in the FRF magnitude of a two-mass system under different viscous friction conditions illustrate this sensitivity to damping characteristics. Moreover, Coulomb friction impacts the low-frequency magnitudes of the FRF, while uncertainties related to the torque constant contribute to overall magnitude fluctuations. Consequently, it becomes apparent that traditional identification methods relying on FRF magnitude are vulnerable to the effects of friction and other disruptive factors.

On the other hand, the resonant and anti-resonant frequencies f_R, f_{AR} are consistent against friction, as shown in the FRF in Fig. 3. Given that inertia parameters can be determined at both resonant and anti-resonant frequencies, their acquisition is feasible without consideration of frictional effects. Therefore, it becomes evident that accurate determination of the inertia matrix of the robot necessitates the utilization of frequency-domain analysis. This approach allows for the identification of parameters independent of friction effects, as resonant and anti-resonant frequencies are solely influenced by inertia and stiffness [17].

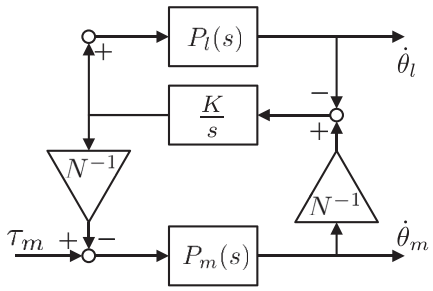

Fig. 4. Block diagram of the dynamics of the flexible joint.

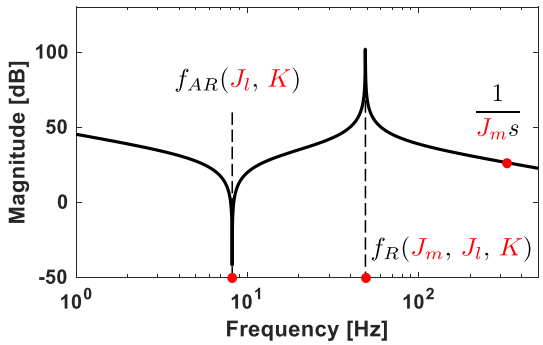

Fig. 5. Frequency response function of two mass system

B. Dynamics Analysis of Flexible Joint Robot

In general, robot dynamics equation is typically modeled under the assumption that the robot joint is rigid. However, in cases where the joint is flexible, it becomes necessary to decompose the dynamics into motor and load sides. This is particularly relevant when the linkage is connected to the motor through a flexible element, including spring or Harmonic Drive. Such a setup results in a two-mass behavior, which can be readily decomposed in the frequency domain, revealing resonance characteristics.

The flexible joint of FJR can be modeled as a two-mass model as following two equations.

$$J_l\ddot{\theta}_l = K\left(\frac{1}{N}\theta_m - \theta_l\right) \tag{1}$$

$$J_m\ddot{\theta}_m = \tau_m - \frac{K}{N}\left(\frac{1}{N}\theta_m - \theta_l\right) \tag{2}$$

The equation (1) and (2) formulate the dynamics of the link side and the motor side, respectively, where J_i and K denote inertia and stiffness. The subscripts l and m denote the load side and the motor side, respectively. This two-mass model can be illustrated as a block diagram in Fig. 4. The presence of elasticity, denoted by K, makes the system prone to resonant behaviors, a phenomenon that becomes notably apparent within the frequency domain. Such a characteristic is advantageous for the parameter identification of flexible joints, enabling the determination of motor inertia, load inertia, and stiffness directly from frequency response data.

III. Nonlinearity-robust multi-DOF Parameter Identification of Flexible Joint Robot

A. Identification of Joint Flexibility based on Resonance Frequency

The block diagram of the two-mass system, shown in Figure 4, can be used to derive the following transfer function from the motor torque τ_m to the motor velocity $\dot{\theta}_m$,as derived in [18].

$$\begin{aligned}\frac{\dot{\theta}_m(s)}{\tau_m(s)} &= \frac{P_m(s+KP_l)}{s+KN^{-2}(s)P_m(s)+KP_l} \\ &= \frac{s^2+\frac{K}{J_l}}{J_m s\left(s^2+K\left(\frac{1}{N^2J_m}+\frac{1}{J_l}\right)\right)},\end{aligned} \tag{3}$$

where $P_m = 1/J_m s$ and $P_l = 1/J_l s$ are the motor side dynamics and the load side dynamics, respectively. The damping term can be disregarded due to its negligible impact on the identification of inertia parameters, as evidenced in Fig. 3. The transfer function in (3) shows that the motor side dynamics $1/J_m s$ become dominant in the high frequency range (where $s \simeq \infty$). This feature can be exploited to identify the motor inertia J_m by investigating the magnitude of the FRF measurements at high frequencies.

Equation (3) also reveals that the resonance frequency ω_R and the anti-resonance frequency ω_{AR} can be derived as below.

$$f_R = \frac{1}{2\pi}\sqrt{\frac{K(N^2J_m+J_l)}{N^2J_mJ_l}}\quad, f_{AR} = \frac{1}{2\pi}\sqrt{\frac{K}{J_l}} \tag{4}$$

These frequencies can be used to identify the load inertia J_l and the stiffness K using the following equations:

$$J_l = \left(\frac{f_R^2}{f_{AR}^2}-1\right)N^2J_m, \tag{5}$$

$$K = 4\pi^2 f_{AR}^2 J_l. \tag{6}$$

Therefore, parameters of the two-mass system can be identified at three red points at Fig. 5, which are robust to nonlinearities.

B. Modeling of Flexible Joint Robot Dynamics

For an n-DOF flexible joint robot with link angle $\boldsymbol{q} \in \mathbb{R}^n$, the dynamic equations can be expressed in relation to the motor angle, motor torque, and the spring stiffness as follows:

$$\boldsymbol{J}(\boldsymbol{q})\ddot{\boldsymbol{q}} + \boldsymbol{C}(\boldsymbol{q},\dot{\boldsymbol{q}}) + \boldsymbol{G}(\boldsymbol{q}) = \boldsymbol{K}(\frac{1}{N}\boldsymbol{\theta} - \boldsymbol{q}) \tag{7}$$

$$\boldsymbol{B}\ddot{\boldsymbol{\theta}} + \boldsymbol{D}\dot{\boldsymbol{\theta}} = \boldsymbol{\tau_m} - \frac{1}{N}\boldsymbol{K}(\frac{1}{N}\boldsymbol{\theta} - \boldsymbol{q}) \tag{8}$$

where (7) and (8) represent the dynamics of robot link and motor, respectively. In (7), $\boldsymbol{J}$, $\boldsymbol{C}$, and $\boldsymbol{G}$ respectively denote the link inertia matrix, Coriolis/centripetal effects, and gravitational effects, while $\boldsymbol{B}, \boldsymbol{D}, \boldsymbol{K}$ in (8) represent the inertia, the damping coefficient, and the stiffness of the motor side, respectively.

With the similarity between these equations and the dynamic model of the two-mass system, as depicted in (1) and

(2), $\boldsymbol{B}$ can be equated with J_m, representing the motor-side inertia values of every joints, while $\boldsymbol{J}$ can be correlated with J_l signifying the link-side inertia values of every joints.

However, the inertia matrix $\boldsymbol{J}(\boldsymbol{q})$ of a multi-DOF robot is dependent on the robot's posture. Thus, it should be noted that the change of effective inertia according to robot's posture, when applying identification of the two-mass system using FRF for the n-DOF robot.

C. Sequential Excitation Algorithm for Inertia Matrix Identification

1) Decomposition of Posture Dependent Inertia Matrix: This paper proposes a method for obtaining the parameter-varying inertia matrix of a rigid body by exploiting its trigonometric structure. The inertia matrix is obtained using the Newton-Euler or Lagrange method and reformulated into two parts: the posture dependent matrix and the constant matrix. The constant part can be identified by measuring the inertia values at several fixed postures. The measured inertia values correspond to the diagonal elements of the inertia matrix. These diagonal elements can be represented as a sinusoidal function of the joint angle.

$$J_{ii}(\boldsymbol{q}) = \sum_{j=i}^{k} \mathcal{C}_{i,j}(\boldsymbol{q})\alpha_{i,j} \tag{9}$$

where $J_{ii}(\boldsymbol{q})$ is a inertia value which affects i-th actuator. In addition, $\mathcal{C}_{i,j}$ is a sinusoidal function, which is subordinated by the joint angle. $\alpha_{i,j}$ is the coefficient specified by a fixed parameter of a robot (mass, length, and so on). k represents the number of angle (q_k) that appears in the element $J_{ii}(q)$.

The equation (9) implies the inertia value J_{ii} consists of trigonometric functions $\boldsymbol{q}$. We reformulate (9) into a linear equation with the trigonometric function part $\boldsymbol{\mathcal{C}}$ and the constant part $\boldsymbol{\alpha}$.

$$J_{ii}(\boldsymbol{\beta}) = \begin{bmatrix}\mathcal{C}_{i,1} & \mathcal{C}_{i,2} & \cdots & \mathcal{C}_{i,k-1} & 1\end{bmatrix} \begin{bmatrix}\alpha_{i,1}\\ \alpha_{i,2}\\ \vdots \\ \alpha_{i,k}\end{bmatrix} \tag{10}$$

where $\boldsymbol{\beta}$ denotes the vector of specific joint angles. To ensure the invertibility of the trigonometric matrix $\boldsymbol{\mathcal{C}}$, we set a appropriate values of vector $\boldsymbol{\beta}$. Measuring the inertia value $J_{ii}(\boldsymbol{\beta})$ allows us to determine the fixed coefficients, α_{ik}. Thus, a equations for $J_{ii}(q)$ that encompasses all joint angles can be obtained.

Consequently, the final matrix equation incorporating k experiments for deriving the constant part is as follows:

$$\underbrace{\begin{bmatrix}\boldsymbol{J}_{ii}^{1}\\ \boldsymbol{J}_{ii}^{2}\\ \vdots \\ \boldsymbol{J}_{ii}^{k-1}\\ \boldsymbol{J}_{ii}^{k}\end{bmatrix}}_{\boldsymbol{J}_{ii}} = \underbrace{\begin{bmatrix}\mathcal{C}_{i,1}^{1} & \mathcal{C}_{i,2}^{1} & \cdots & \mathcal{C}_{i,k-1}^{1} & 1\\ \mathcal{C}_{i,1}^{2} & \mathcal{C}_{i,2}^{2} & \cdots & \mathcal{C}_{i,k-1}^{2} & 1\\ \vdots & \vdots & \ddots & \vdots & \vdots\\ \mathcal{C}_{i,1}^{k-1} & \mathcal{C}_{i,2}^{k-1} & \cdots & \mathcal{C}_{i,k-1}^{k-1} & 1\\ \mathcal{C}_{i,1}^{k} & \mathcal{C}_{i,2}^{k} & \cdots & \mathcal{C}_{i,k-1}^{k} & 1\end{bmatrix}}_{\boldsymbol{\mathcal{C}}_i} \underbrace{\begin{bmatrix}\alpha_{i,1}\\ \alpha_{i,2}\\ \vdots \\ \alpha_{i,k-1}\\ \alpha_{i,k}\end{bmatrix}}_{\boldsymbol{\alpha}_i}, \tag{11}$$

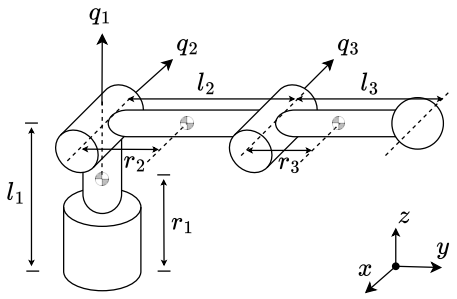

Fig. 6. Structure of 3-DOF manipulator

where $\boldsymbol{\mathcal{C}}_i \in \mathbb{R}^{k\times k}$ is an invertible matrix whose rows consist of trigonometric function term with each robot posture. $\boldsymbol{J}_{ii} \in \mathbb{R}^k$ is set of inertia matrix at each posture estimated with FRF. Finally, the constant vector utilized to determine the inertia matrix is derived as $\boldsymbol{\alpha_i} = \boldsymbol{\mathcal{C}}_i^{-1}\boldsymbol{J}_{ii}$.

2) Case Study with 3-DOF Manipulator: We consider a rigid-body-based manipulator equipped with three degrees of freedom (DOF), arranged in a yaw-pitch-pitch sequence of joint configurations, as illustrated in Fig. 6. The inertia matrix of this setup is articulated as follows [19].

$$\boldsymbol{J}(q) = \begin{bmatrix}J_{11}(q) & 0 & 0\\ 0 & J_{22}(q) & J_{23}(q)\\ 0 & J_{32}(q) & J_{33}(q)\end{bmatrix} \tag{12}$$

Each component is given as

$$\begin{aligned} J_{11}(\boldsymbol{q}) =& I_{z1} + I_{y2}s_2^2 + I_{y3}s_{23}^2 + I_{z2}c_2^2 + I_{z3}c_{23}^2 \\ &+ m_2 r_2^2 c_2^2 + m_3(l_2c_2 + r_3c_{23})^2 \end{aligned} \tag{13}$$

$$\begin{aligned} J_{22}(\boldsymbol{q}) =& I_{x2} + I_{x3} + m_3 l_2^2 + m_2 r_2^2 + m_3 r_3^2 \\ &+ 2m_3 l_2 r_3 c_3 \end{aligned} \tag{14}$$

$$J_{33}(\boldsymbol{q}) = I_{x3} + m_3 r_3^2 \tag{15}$$

$$J_{23}(\boldsymbol{q}) = J_{32}(q) = I_{x3} + m_3 r_3^2 + m_3 l_2 r_3 c_3, \tag{16}$$

where I_{ij} denotes the inertia along the i-axis of j-th link, and m_j, l_j, r_j represent mass, length, and center of mass of j-th link, respectively. Hereafter, abbreviations c_2 and c_{23} will be employed to represent $\cos(q_2)$ and $\cos(q_2 + q_3)$, respectively.

By applying $s_o^2 = 1 - c_o^2$ to each of the inertia functions, the following can be derived:

$$J_{11}(\boldsymbol{q}) = \alpha_{11}c_{23}^2 + \alpha_{12}c_2^2 + \alpha_{21}c_2c_{23} + \alpha_{13} \tag{17}$$

$$J_{22}(\boldsymbol{q}) = 2\alpha_{21}c_3^2 + \alpha_{22} \tag{18}$$

$$J_{33}(\boldsymbol{q}) = \alpha_{31} \tag{19}$$

$$J_{23}(\boldsymbol{q}) = J_{32}(\boldsymbol{q}) = \alpha_{21}c_3^2 + \alpha_{31} \tag{20}$$

As shown in (19), the inertia value of the most distal joint remains constant, since there is no variation in inertia corresponding to changes in joint configuration for the last actuator. Conversely, for the second joint, inertia variations are dependent on angular changes in the third actuator, as depicted in (18). Thus, to derive the inertia function of the second actuator, two distinct sets of experimental data

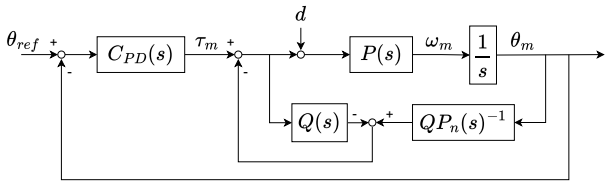

Fig. 7. Block diagram of DOB with PD position control

are required that can differentiate the influence of c_3 in the second joint. Lastly, the first joint is influenced by the angular changes of both the second and the third actuators. As shown in (17), while the inertia of the first actuator has four coefficients, it is feasible to obtain $\boldsymbol{\mathcal{C}}_1$, satisfying the minimum rank requirement for inversion, by utilizing the coefficients acquired from (18). Examining the equations from (17) to (20), the sequential excitation algorithm is suggested as follows:

1) The inertia values are obtained sequentially, starting from the most distal third joint, proceeding to the second, and finally the first joint, while conducting FRF measurements at each stage.
2) In the case of J_{11}, J_{22}, and J_{23}, which exhibit angle dependency, a few angle values are fixed and perturbations are introduced to induce movements in their vicinity, thereby preserving linearity within a certain range during FRF measurements.
3) By conducting FRF measurements at a sufficiently large number of fixed angle values, it is possible to extract the complete mathematical models for coefficients α_{11} to α_{31} in the equations for J_{11}, J_{22}, and J_{23}.

$$\begin{bmatrix} J_{11}^1 \\ J_{11}^2 \\ J_{11}^3 \end{bmatrix} = \boldsymbol{\mathcal{C}}_1 \begin{bmatrix} \alpha_{11} \\ \alpha_{12} \\ \alpha_{13} \end{bmatrix} \tag{21}$$

By setting the angles to secure a fixed posture of the robot, it allows $\boldsymbol{\mathcal{C}}_1$ to form a triangular matrix. In this triangular matrix, the diagonal matrix is an identity matrix, which offers computational benefits when calculating the inverse matrix. J_{22} can be calculated using the same method as described above. Note that experiment for non-diagonal term J_{23} is not necessary since α_{21} and α_{31} can be obtained from other experiments.

This is the proposed sequential excitation algorithm to determine the inertia matrix based on a multitude of FRF. Each individual FRF measurement is conducted by applying a torque input to the i-th joint using a multi-sine signal and subsequently measuring the corresponding joint's motor velocity. Following this, the FRF between the input and output is extracted and fitted to the two-mass model to ascertain parameters such as J_m, K, and J_l. From these parameters, the J_l values are isolated and utilized in the aforementioned process to compute the inertia matrix.

D. Disturbance Observer for Ensuring Non-exciting Link as Rigid Body

This paper proposed a process to determine the posture dependent inertia matrix of an FJR by integrating frequency

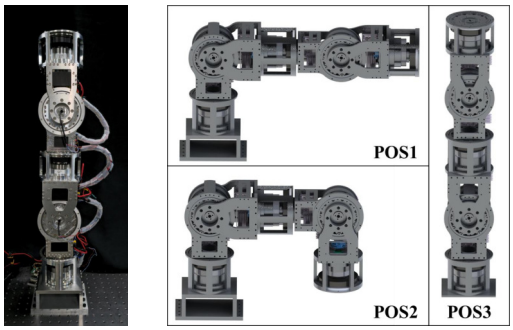

(a) (b)

Fig. 8. (a) Experiment setup (b) Postures for identification

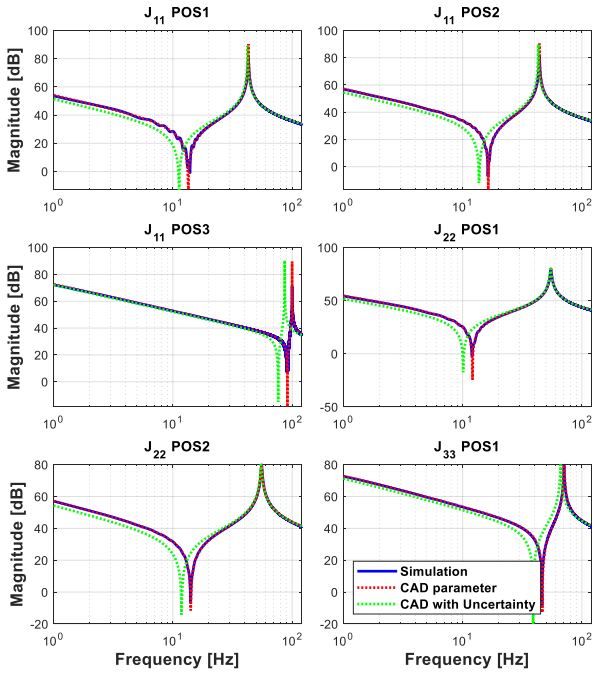

Fig. 9. FRF from simulation and with inertia uncertainty

response analyses at specific postures. During the posture specification process, it is necessary to impose control to fix the position of joints that are not being excited to prevent movement. If the implemented controller is set to have low stiffness, it results in the associated joint experiencing concurrent vibrations, generating undesirable inertia effect.

Therefore, to rigidly fix the unexcited actuators, Disturbance Observer (DOB) and PD control are applied, as illustrated in Fig. 7. Each of the unexcited actuators is controlled by a DOB to reject disturbances induced by excitations, thereby rigidly anchoring them. The nominal model $P_n(s)$ is utilized as the two-mass system model with (3), wherein the parameters incorporated naturally emerge during the process of determining the inertia matrix of the terminal link of the respective joint. Finally, the proposed sequential excitation algorithm of obtaining the inertia matrix of the n-DOF FJR as outlined in this section is depicted in Fig. 1.

IV. Verification

The methodology for obtaining the inertia matrix was validated through simulation and experiment with the robot

TABLE I

SIMULATION RESULT

Posture	POS1			POS2		POS3
$[\mathrm{kg}\cdot\mathrm{m}^2]$	J_{11}	J_{22}	J_{33}	J_{11}	J_{22}	J_{11}
J_l	0.6987	0.6929	0.0466	0.696	0.5072	0.0152
J_{CAD}	0.6987	0.6929	0.0466	0.696	0.5072	0.0152
$[\mathrm{kg}\cdot\mathrm{m}^2]$	α_{11}	α_{12}	α_{13}	α_{21}	α_{22}	α_{31}
Simulation	0.1362	0.4544	0.0152	0.0928	0.5072	0.0466
CAD	0.1362	0.4544	0.0152	0.0928	0.5072	0.0466
with uncertainty	0.1946	0.6492	0.0217	0.1326	0.7246	0.0666
Error(%)	29.99	30.01	29.95	30.04	30.00	35.74

[20]. Both validations use the postures of the robot, set as [POS1 : $q_2 = q_{23} = 0$; POS2 : $q_2 = 0$, $q_{23} = -\pi/2$; POS3 : $q_2 = q_{23} = \pi/2$.], illustrated at Fig. 8. In addition, the same method was applied to calculate the inertia matrix for the actual manipulator, which was then compared with CAD data for analysis.

A. Simulation: Theory vs CAD

Before applying the proposed algorithm to the actual robot, its logic and functionality were verified through simulation. The simulation was conducted using Matlab Simscape Multibody Link, and the 7-DOF manipulator [20] was utilized. Among the 7-DOF, the 3rd, 4th, and 6th joints only were utilized with 3-DOF. The joints were established as a flexible joint with motors and spring models (derived from Harmonic Drive). The remaining joints were constrained in the simulation to mimic the yaw-pitch-pitch 3-DOF manipulator structure discussed in this paper.

First, FRF was conducted starting from the most distal joint. For the excitation signal of FRF, a Schroder multi-sine [12] with frequency components ranging from 0.1 to 120Hz was applied to the motor. The velocity of the motor was then measured to obtain the FRF of (3). Subsequently, the method outlined in Section III-A was employed to decompose the motor inertia and load inertia, resulting in the determination of J_l for each joint.

Fig. 9 illustrates a comparison between the FRFs obtained from simulation results and those computed from CAD values. The resonance and anti-resonance frequencies of both FRFs align accurately, as further confirmed by the identical corresponding J_l values, as depicted in Table I. This result suggests that the decomposed load inertia J_l at the flexible joint corresponds to an element of the inertia matrix J_{ii}.

Additionally, the impact of uncertainty in load inertia was examined through simulations. The green dots in Fig. 9 represent the FRFs extracted with about 30% discrepancy in load inertia values compared to those in CAD. As anticipated from (4), it was observed that as the load inertia increased, the anti-resonance frequencies decreased. Furthermore, when comparing the resulting α_{ik} values obtained from CAD with those calculated based on the corresponding load inertia, a similar level of error (30%) was observed in the α_{ik} values.

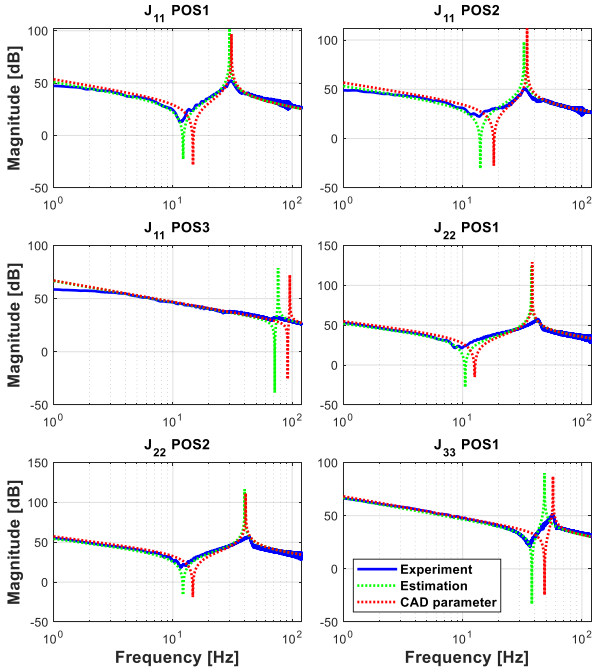

Fig. 10. FRF from experiment and CAD parameters

TABLE II

EXPERIMENT RESULT

Posture	POS1			POS2		POS3
	J_{11}	J_{22}	J_{33}	J_{11}	J_{22}	J_{11}
$J_{ii}[\mathrm{kg}\cdot\mathrm{m}^2]$	0.9381	0.92	0.07	0.57	0.6242	0.0223
$K[\mathrm{Nm/rad}]$	5500	4500	4500	4000	4000	4000
$[\mathrm{kg}\cdot\mathrm{m}^2]$	α_{11}	α_{12}	α_{13}	α_{21}	α_{22}	α_{31}
CAD	0.1362	0.4544	0.0152	0.0928	0.5072	0.0466
Experiment	0.2202	0.5477	0.0223	0.1479	0.6242	0.07
Error(%)	38.15	17.03	31.84	37.25	18.74	38.86

B. Experiment: Inertia Matrix Identification

1) Set-up: The experiments were conducted using the same robot model employed in the simulation. However, to bring the structure of the yaw-pitch-pitch 3-DOF manipulator discussed in this paper, we omitted the two lower joints and constrained the 5th joint using DOB and PD control. J_{ii} obtained from each posture are illustrated in Fig. 8. The excitation signal used in the experiment was a Schröder multisine with frequency components ranging from 0.1 to 120Hz.

2) Experiment Result: FRF for each posture of the robot are depicted in Fig. 10. The blue, green, and red data were derived from experimental data, estimated J_{ii} values, and CAD parameters, respectively. The observed discrepancies at lower frequencies can be attributed to the absence of damping terms in the modeled transfer function for both motor and load sides, as outlined in (3). The proposed algorithm concentrates on the resonance and anti-resonance frequencies, which remain unaffected by friction. Therefore, the damping term can be ignored due to its negligible impact in resonances. Based on the experimental results, the esti-

mated J_{ii} values and their associated calculated α_{ik} values were determined. Additionally, the stiffness K, derived from the dynamics of a two-mass system (6), is also presented in Table II.

As indicated by the table, the α_{ik} values within the inertia matrix, obtained through the proposed method, show a similar pattern to those derived from CAD data, with an observed average error of 30.31%. This error can also be observed in Fig. 10, through the comparison between the FRF derived from CAD parameters (red) and those obtained from experimental data (blue), indicating a similar result observed in the simulation with inertia uncertainty as well. Such observations suggest that CAD parameters may not accurately reflect the actual inertia parameters of the robot. Notably, the experimental values consistently exceed those predicted by CAD data, hinting at potential inaccuracies within the CAD values themselves. Factors contributing to this variance may include the omission of real-world elements such as wires in CAD models. Additionally, the physical properties of components such as motors, encoders, and harmonic drives might not have been fully accounted for, leading to discrepancies in the actual inertia values observed. Meanwhile, the stiffness K is well estimated compared with the specification of the Harmonic Drive.

V. Conclusion and Future Work

This paper presents the sequential excitation algorithm for deriving the inertia matrix of a Flexible Joint Robot (FJR) utilizing the Frequency Response Function (FRF). This approach eliminates the need of complex theories or optimization. It is investigated how frequency-based identification attenuates the effect of the position-dependent friction by constant velocity control experiment. Furthermore, its effectiveness for identifying the inertia matrix of flexible joint was verified. Finally, the algorithm for deriving the inertia matrix of the FJR was developed based on a two-mass system model.

The validity of the proposed algorithm was verified through simulation. The identified inertia matrix was compared with the one derived from CAD parameters. Through FRF analysis, it was demonstrated that the inertia matrix of the flexible joint robot could be determined by effectively decoupling motor inertia and load inertia, utilizing the J_l values of the two-mass system. A significant difference was observed between the the experiment and the CAD-derived inertia matrices, highlighting the importance of acquiring system parameters through experiments, rather than solely relying on CAD values.

Throughout this process, the advantages and necessity of frequency domain analysis for flexible joints are emphasized. Furthermore, the proposed algorithm is introduced that extends the applicability of the FRF-based parameter identification method to obtain position dependent inertia matrix with nonlinearity robustness.

This paper exclusively focuses on manipulators with a 3-DOF joint configuration in the order of yaw, pitch, and pitch. Generalized algorithms for different structures or those with a higher degree of freedom are planned for future research.

References

[1] D. Lee, J. Back, and S. Oh, "Workspace nonlinear disturbance observer for robust position control of flexible joint robots," *IEEE Robotics and Automation Letters*, pp. 1–8, 2024.

[2] A. De Luca and W. J. Book, "Robots with flexible elements," *Springer Handbook of Robotics*, pp. 243–282, 2016.

[3] A. Albu-Schäffer, S. Haddadin, C. Ott, A. Stemmer, T. Wimböck, and G. Hirzinger, "The dlr lightweight robot: design and control concepts for robots in human environments," *Industrial Robot: an international journal*, vol. 34, no. 5, pp. 376–385, 2007.

[4] K. Yuki, T. Murakami, and K. Ohnishi, "Vibration control of a 2 mass resonant system by the resonance ratio control," *IEEJ Transactions on Industry Applications*, vol. 113, no. 10, pp. 1162–1169, 1993.

[5] H. Lee, J. Lee, M. Keppler, and S. Oh, "Robust elastic structure preserving control for high impedance rendering of series elastic actuator," *IEEE Robotics and Automation Letters*, vol. 9, no. 4, pp. 3601–3608, 2024.

[6] M. Zinn, O. Khatib, B. Roth, and J. K. Salisbury, "Playing it safe [human-friendly robots]," *IEEE Robotics & Automation Magazine*, vol. 11, no. 2, pp. 12–21, 2004.

[7] S. Robla-Gómez, V. M. Becerra, J. R. Llata, E. Gonzalez-Sarabia, C. Torre-Ferrero, and J. Perez-Oria, "Working together: A review on safe human-robot collaboration in industrial environments," *Ieee Access*, vol. 5, pp. 26 754–26 773, 2017.

[8] J. Swevers, W. Verdonck, and J. De Schutter, "Dynamic model identification for industrial robots," *IEEE control systems magazine*, vol. 27, no. 5, pp. 58–71, 2007.

[9] C. Gaz, M. Cognetti, A. Oliva, P. Robuffo Giordano, and A. De Luca, "Dynamic identification of the franka emika panda robot with retrieval of feasible parameters using penalty-based optimization," *IEEE Robotics and Automation Letters*, vol. 4, no. 4, pp. 4147–4154, 2019.

[10] C. Rucker and P. M. Wensing, "Smooth parameterization of rigid-body inertia," *IEEE Robotics and Automation Letters*, vol. 7, no. 2, pp. 2771–2778, 2022.

[11] J. Swevers, C. Ganseman, D. B. Tukel, J. De Schutter, and H. Van Brussel, "Optimal robot excitation and identification," *IEEE transactions on robotics and automation*, vol. 13, no. 5, pp. 730–740, 1997.

[12] R. Pintelon and J. Schoukens, *System identification: a frequency domain approach*. John Wiley & Sons, 2012.

[13] M. Östring, S. Gunnarsson, and M. Norrlöf, "Closed-loop identification of an industrial robot containing flexibilities," *Control Engineering Practice*, vol. 11, no. 3, pp. 291–300, 2003, advances in Automotive Control. [Online]. Available: https://www.sciencedirect.com/science/article/pii/S0967066102001144

[14] E. Wernholt and S. Gunnarsson, "On the use of a multivariable frequency response estimation method for closed loop identification," in *2004 43rd IEEE Conference on Decision and Control (CDC) (IEEE Cat. No.04CH37601)*, vol. 1, 2004, pp. 827–832 Vol.1.

[15] ——, "Nonlinear grey-box identification of industrial robots containing flexibilities," *IFAC Proceedings Volumes*, vol. 38, no. 1, pp. 356–361, 2005, 16th IFAC World Congress.

[16] S. A. Zimmermann, M. Enqvist, S. Gunnarsson, S. Moberg, and M. Norrlöf, "Experimental evaluation of a method for improving experiment design in robot identification," in *2023 IEEE International Conference on Robotics and Automation (ICRA)*, 2023, pp. 11 432–11 438.

[17] S. E. Saarakkala, T. Leppinen, M. Hinkkanen, and J. Luomi, "Parameter estimation of two-mass mechanical loads in electric drives," in *2012 12th IEEE International Workshop on Advanced Motion Control (AMC)*, 2012, pp. 1–6.

[18] S. Oh and K. Kong, "High-precision robust force control of a series elastic actuator," *IEEE/ASME Transactions on Mechatronics*, vol. 22, no. 1, pp. 71–80, 2017.

[19] R. M. Murray, Z. Li, S. S. Sastry, and S. S. Sastry, *A mathematical introduction to robotic manipulation*. CRC press, 1994.

[20] D. Lee, K. Choi, J. Kim, W. Yun, T. Kim, K. Nam, and S. Oh, "Exsler: Development of a robotic arm for human skill learning," in *2023 IEEE/ASME International Conference on Advanced Intelligent Mechatronics (AIM)*, 2023, pp. 209–214.